EARTHQUAKE ENGINEERING AND STRUCTURAL DYNAMICS
Earthquake Engng Struct. Dyn. 2010; **39**:1421–1442
Published online 20 September 2010 in Wiley Online Library (wileyonlinelibrary.com). DOI: 10.1002/eqe.1038

Seismic performance assessment of base-isolated safety-related nuclear structures

Yin-Nan Huang[1,*,†], Andrew S. Whittaker[2] and Nicolas Luco[3]

[1]*School of Civil and Environmental Engineering, Nanyang Technological University, N1-01c-76, 50 Nanyang Ave., Singapore 639798, Singapore*
[2]*Department of Civil, Structural and Environmental Engineering, University at Buffalo, State University of New York, Buffalo, NY 14260, U.S.A.*
[3]*United States Geological Survey, Denver, CO 80225, U.S.A.*

SUMMARY

Seismic or base isolation is a proven technology for reducing the effects of earthquake shaking on buildings, bridges and infrastructure. The benefit of base isolation has been presented in terms of reduced accelerations and drifts on superstructure components but never quantified in terms of either a percentage reduction in seismic loss (or percentage increase in safety) or the probability of an unacceptable performance. Herein, we quantify the benefits of base isolation in terms of increased safety (or smaller loss) by comparing the safety of a sample conventional and base-isolated nuclear power plant (NPP) located in the Eastern U.S. Scenario- and time-based assessments are performed using a new methodology. Three base isolation systems are considered, namely, (1) Friction Pendulum^{TM} bearings, (2) lead–rubber bearings and (3) low-damping rubber bearings together with linear viscous dampers. Unacceptable performance is defined by the failure of key secondary systems because these systems represent much of the investment in a new build power plant and ensure the safe operation of the plant. For the scenario-based assessments, the probability of unacceptable performance is computed for an earthquake with a magnitude of 5.3 at a distance 7.5 km from the plant. For the time-based assessments, the annual frequency of unacceptable performance is computed considering all potential earthquakes that may occur. For both assessments, the implementation of base isolation reduces the probability of unacceptable performance by approximately four orders of magnitude for the same NPP superstructure and secondary systems. The increase in NPP construction cost associated with the installation of seismic isolators can be offset by substantially reducing the required seismic strength of secondary components and systems and potentially eliminating the need to seismically qualify many secondary components and systems.

Received 7 January 2010; Revised 13 April 2010; Accepted 7 June 2010

KEY WORDS: nuclear power plant; base isolation; risk assessment; fragility curve; ground motion scaling; secondary system

*Correspondence to: Yin-Nan Huang, School of Civil and Environmental Engineering, Nanyang Technological University, N1-01c-76, 50 Nanyang Ave., Singapore 639798, Singapore.
†E-mail: ynhuang@ntu.edu.sg

1. INTRODUCTION

Seismic or base isolation is a proven technology for reducing the effects of earthquake shaking on buildings, bridges and infrastructure [1, 2]. Base isolation has been implemented in safety-related nuclear structures in France and South Africa [3], but the principles and materials used there differ from those used in design practice in North America. Although the benefits of base isolation are understood well in terms of reduced seismic demands on structural and nonstructural components and systems in nuclear power plants (NPPs) [3–8], these benefits have not been quantified in terms of either percentage change in vulnerability or a reduction in the probability of unacceptable performance given a seismic hazard.

Since 1991, the U.S. Nuclear Regulatory Commission (NRC) has required all utilities in the U.S. to examine the seismic risk of their NPPs [9]. The NRC identify Seismic Margin Assessment (SMA) and Seismic Probabilistic Risk Assessment (SPRA) as acceptable methodologies for this examination [10]. SMA determines a high-confidence-low-probability-of-failure (HCLPF) capacity as the seismic margin of a plant [11–13]. SMA is less computationally intensive than SPRA but cannot be used to estimate the annual frequency of core damage, which is a product of SPRA. Information on SPRA procedures can be found in Smith *et al.* [14], NUREG/CR-2300 [15], and Reed and Kennedy [16].

Huang *et al.* [17] proposed a new seismic performance assessment methodology based on existing SPRA procedures [14, 16, 17] and tools under development for the performance-based design of buildings. The new methodology, which is briefly summarized in Section 2, uses response-based rather than ground-motion-based parameters to characterize fragility curves for structural components and secondary components and systems in an NPP; scales ground motions for response-history analysis based on the seismic hazard at the fundamental period of the NPP rather than peak ground acceleration; and directly considers the correlation in the responses of NPP components for risk computations.

Herein, we quantify the benefits of base isolation for an NPP located on a rock site in the Eastern U.S. using the assessment methodology of Huang *et al.* [17]. Scenario-earthquake and time-based assessments are presented to enable a comparison of the seismic vulnerability of the conventionally constructed and base-isolated NPP and thus quantify the benefit of isolation in terms of increased seismic safety. The assessment focuses on secondary systems in a sample NPP since these systems represent much of the investment in a new build power plant and the failure of these systems affects the safe operation of the plant.

A perceived shortcoming with the use of base isolation for safety-related nuclear structures is increased construction cost with respect to conventional construction. This increase in construction cost could be offset by substantial reductions in the required seismic strength of secondary components and systems and by potentially eliminating the need to seismically qualify many secondary components and systems. We use the methodology of Huang *et al.* to quantify the possible reductions in required seismic strength of secondary components and systems for the sample NPP and site.

Section 2 summarizes the seismic performance methodology used in the study. Section 3 introduces the sample nuclear reactor building and site used for the performance assessments. The site was chosen because most of the proposed new build NPPs in the U.S. are located in the Eastern U.S. Sections 4 (Scenario-based assessment) and 5 (Time-based assessment) present results of the performance assessments that enable the reader to quantify the benefits of base isolation in terms of either increased seismic safety or reductions in required seismic strength of secondary components and systems.

DOI: 10.1002/eqe

2. SEISMIC PERFORMANCE ASSESSMENT METHODOLOGY

The methodology proposed in Huang *et al.* [17] for probabilistic seismic performance assessment of NPPs can be used to perform three types of assessment, namely, intensity-, scenario- and time-based assessments.

An intensity-based performance assessment estimates the probability of unacceptable performance, given that the NPP experiences a specific intensity of shaking, such as that represented by a Safe-Shutdown-Earthquake (SSE) response spectrum. A scenario-based performance assessment estimates the probability of unacceptable performance, given that an NPP experiences a specific earthquake, defined as a combination of earthquake magnitude and distance of the site from the part of the fault on which the earthquake occurs. The seismic hazard is characterized by a distribution of spectral demand predicted by an attenuation relationship for the combination of magnitude and distance. A time-based assessment estimates the annual frequency of unacceptable performance of an NPP, considering all potential earthquakes that may occur. The seismic hazard is characterized by seismic hazard curves at a period of interest. A time-based assessment is performed as a series of intensity-based assessments with different target spectral intensities determined from the seismic hazard curve.

Figure 1 presents the five steps of the methodology of Huang *et al.* Step 1 of the Huang procedure requires the user to develop fragility curves for the structural and nonstructural components of the NPP, as well as fault trees and event trees to identify possible accident sequences that could contribute to unacceptable performance, such as core melt and radiation release. Step 2 characterizes the seismic hazard using a design spectrum, a distribution of spectral demand for a combination of magnitude and distance and seismic hazard curves for intensity-, scenario- and time-based assessments, respectively. Step 3 performs response-history analysis of the NPP subjected to the seismic hazard of Step 2 to estimate the accelerations, forces, displacements and deformations that serve as demands on the NPP's components and contents. Damage of the structural and nonstructural components is assessed in Step 4 using the demands computed in Step 3 and fragility curves developed in Step 1. Step 5 computes seismic risk using the results of Step 4 and the accident sequences developed in Step 1. The product of Step 5 for intensity- and scenario-based assessments is the probability of unacceptable performance for the NPP subjected to the given seismic hazard and that for time-based assessment is the annual frequency of unacceptable performance.

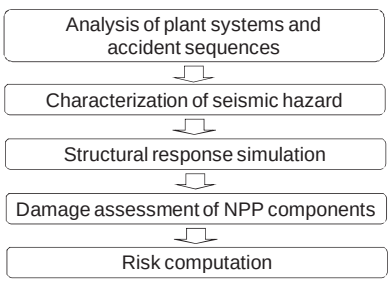

Figure 1. The procedure of seismic performance assessment of NPPs.

DOI: 10.1002/eqe

3. SAMPLE NUCLEAR REACTOR BUILDINGS

3.1. Conventional reactor building

Figure 2 presents a cutaway view of the sample NPP reactor building analyzed in this study. A lumped-mass stick model of this reactor building, shown in Figure 3(a), is developed in the computer code SAP2000 [18] for response-history analysis. The model is composed of two sticks: one representing the (external) containment structure and the other representing the internal structure. The two sticks are structurally independent and connected only at the base. The properties of the sticks are back-calculated from analysis of a 3-D reactor building, provided by a Nuclear Steam Supply System (NSSS) vendor, using industry-standard procedures. The mass of the structure and the secondary systems is lumped at discrete locations at key levels in the reactor building. The discrete masses are connected to the frame elements through rigid links to account for torsional effects. The first mode period of the containment (internal) structure is approximately 0.2 (0.14) s in both horizontal directions (termed as X and Y directions hereafter). The total weight (W) of the NPP reactor building is approximately 75 000 tons.

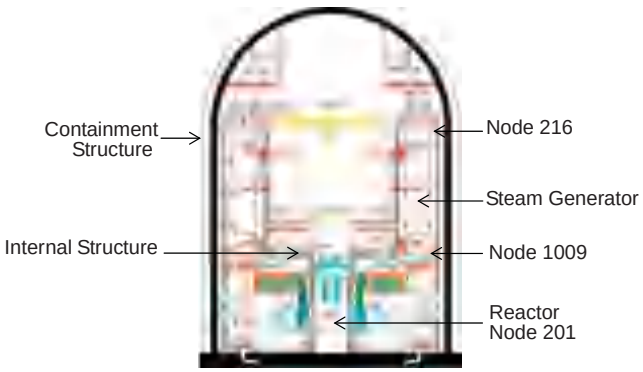

Figure 2. A cutaway view of the sample NPP reactor building.

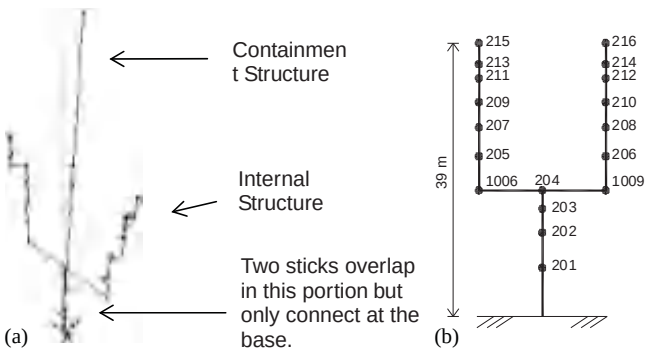

Figure 3. Stick model for the sample NPP reactor building: (a) Model 1 and first mode shape in SAP2000 and (b) stick model.

DOI: 10.1002/eqe

In the lumped-mass stick model of Figure 3(a), the containment structure is assumed to remain elastic since (a) this study focuses on important secondary systems, most of which are supported by the internal structure; and (b) containment structures are designed for large internal pressures (up to 500 kPa) resulting from a postulated accident, and seismic loadings generally do not control their design. Bilinear shear hinges with 3% post-yield stiffness are assigned to all frame elements in the internal structure. The yield shear strengths of the bilinear shear hinges are estimated as $0.5\sqrt{f'_c}A_S$ [19], where f'_c is the compressive strength of concrete with a value of $35\,\mathrm{N/mm^2}$ and A_s is the shear area of each internal-structure stick provided by the supplier of the sample NPP. Design seismic demands on the internal structure are computed for the SSE spectrum, which is a uniform risk spectrum with a mean annual frequency of exceedance (MAFE) of 10^{-5} for the sample NPP site. See Huang *et al.* [17] for more information.

3.2. Base-isolated reactor buildings

Four numerical models of base-isolated reactor buildings are developed in SAP2000 to quantify the effect of implementing base isolation on the seismic vulnerability of secondary systems in the sample NPP reactor building. Model 1 is the conventionally framed NPP reactor building. Models 2 and 3 include representations of Friction Pendulum^{TM} (FP) bearings and lead–rubber (LR) bearings, respectively. Low-damping rubber (LDR) bearings and linear viscous dampers (LVD) provide the isolation system in Model 4. Each base isolation system is modeled using a one-joint link element attached to the bottom of the superstructure. Model 1 is used for the superstructure of Models 2, 3 and 4. Table I lists the properties of the isolation systems for each model.

Bilinear plasticity elements are used to model the LR bearings. Figure 4 illustrates the key variables defining the bilinear hysteresis loop. For FP bearings, the velocity dependence of the coefficient of sliding friction is given by [20, 21]

$$\mu = \mu_{\max} - (\mu_{\max} - \mu_{\min}) \cdot e^{-\alpha V} \tag{1}$$

where μ is the coefficient of sliding friction, varying between $\mu_{\max}$ and $\mu_{\min}$ (obtained at high and very small velocities, respectively), α is a velocity-related parameter and V is the sliding velocity.

Table I. Description of response-history-analysis models.

Model	Protective system	Description*
1	None	First mode periods of the containment and internal structures, in each horizontal direction, are (0.22 s, 0.21 s) and (0.14 s, 0.13 s), respectively
2	Friction Pendulum^{TM} (FP)	$\mu_{\max}=0.06$; $\mu_{\min}=0.03$; $a=55\,\mathrm{s/m}$; $T_d=2\,\mathrm{s}$; $u_y=1\,\mathrm{mm}$
3	Lead–rubber (LR)	$Q_d=0.06\,\mathrm{W}$; $T_d=2\,\mathrm{s}$; $K_u=10K_d$
4	Low-damping rubber (LDR) and linear viscous damper (LVD)	$T_i=2\,\mathrm{s}$; $\beta_i=0.10$

*See Figure 4 for definitions of Q_d, K_u, K_d and u_y. Period T_d is related to K_d through the supported weight; T_i is the isolated period for the LDR isolation systems based on a rigid superstructure and β_i is the damping contributed by LVDs.

DOI: 10.1002/eqe

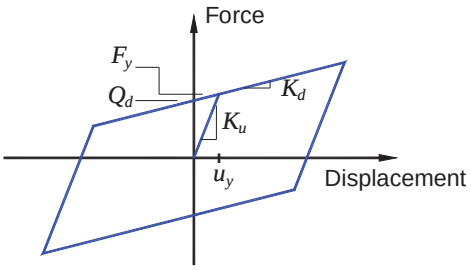

Figure 4. Assumed properties of LR and Coulomb-friction-FP bearings.

Table II. Node numbers and elevations for the supports of key secondary systems in the internal structure of the sample NPP building.

Secondary system	Node number	Elevation (m)
Reactor assembly	201	7
Steam generators	1006, 1009	18
Emergency coolant injection (ECI) tanks	1006, 1009	18
Main steam lines	215, 216	39
Heat transport system (HTS)	1006, 1009	18

A value of $\beta = 55\,\mathrm{s/m}$ is adopted for the study described herein.[‡] The characteristic strength, Q_d of Figure 4, is set equal to 6% of the supported weight W for the LR bearings and μ_{max} is set equal to 6% for the FP bearings, where for Coulomb friction, $Q_d = \mu_{max} W$. The second-slope period (related to K_d of Figure 4 through the supported weight) is assigned a value of 2 s for the LR and FP bearings. The LDR bearings are modeled as linear elements, which is a most reasonable assumption up to shear strains of 200% for many natural rubbers.[§] Model 4 is assigned an isolated period of 2 s with supplemental viscous damping of 10% of critical.

The models of the isolators are deterministic and their mechanical properties are assumed not to change during earthquake shaking due to repeated cycling. Although these intra-event changes in mechanical properties can now be traced over the course of an earthquake [22, 23], their inclusion in this study is not considered central to its purpose. A procedure to address the variation in mechanical properties of isolators for the performance assessment of base-isolated NPPs can be found in [24].

3.3. Key secondary systems and their fragility curves

Table II identifies five key secondary systems in the sample reactor building of Figure 2, including the reactor, steam generators, emergency coolant injection (ECI) tanks, main steam lines and heat transport system (HTS). These secondary systems are attached to the internal structure and are supported at elevations of 7 (Node 201), 18 (Nodes 1006 and 1009) and 39 m (Nodes 215 and

[‡]The hysteresis loop for the FP bearing will converge to the bilinear loop shown in Figure 4 for Coulomb friction ($\beta = \infty$).

[§]The maximum displacement of the isolators computed in this study for the rock site in the Central and Eastern U.S. (CEUS) is 25 cm, which will correspond to a shear strain much less than 100% for prototype isolators for NPP applications.

DOI: 10.1002/eqe

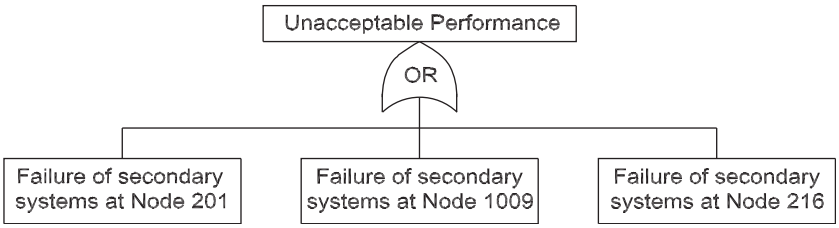

Figure 5. The fault tree for the studies presented in this paper.

216) (see Table II). The node numbers assigned to the internal structure of the sample NPP are presented in Figure 3(b). In this study, we focus on the secondary systems at Nodes 201, 1009 and 216 and define the unacceptable performance of the sample NPP as the failure of *any* of the key secondary systems at Nodes 201, 1009 and 216. This definition is illustrated in Figure 5 using a fault tree, where three failure events are linked to the unacceptable performance through an 'OR' gate.[¶] The probability of unacceptable performance for each of Models 1–4 subjected to a specific seismic hazard is computed to identify the impact of base isolation systems.

For the seismic performance assessment of a safety-related nuclear structure, fragility curves are required for all basic failure events at the lowest level of each fault tree. For this study, the basic failure events are the failure of the secondary systems at Nodes 201, 1009 and 216 and the demand parameter used to develop the fragility curves for the secondary systems is average floor spectral acceleration (AFSA) over a frequency range from 5 to 33 Hz. This demand parameter is chosen since seismic demands on secondary systems in safety-related nuclear structures are characterized typically using a floor response spectrum and the frequencies of most secondary systems range between 5 and 33 Hz. (For a project-specific application, the demand parameter for an NPP component should be selected as the response that governs the failure of that component and fragility curves would have to constructed for that parameter.) A fragility curve can be defined by a median value and a logarithmic standard deviation. Figure 6 presents the three fragility curves used in this study to represent the capacities of the secondary systems at Nodes 201, 1009 and 216, respectively. The median AFSA values are 2.26, 3.15 and 7.02 g for the curves for Nodes 201, 1009 and 216, respectively, and the logarithmic standard deviation for the three curves is 0.43. The median values are estimated assuming that the HCLPF capacity for the secondary systems at a node is no less than the SSE demand at the node. The logarithmic standard deviations are based on the recommendations of Kennedy and Ravindra [25]. More information on the development of the fragility curves of Figure 6 can be found in Huang *et al.* [17].

4. SCENARIO-BASED ASSESSMENT

Step 1 for both the scenario- and time-based assessments is not presented since the fault tree and fragility curves are given in Figures 5 and 6, respectively.

[¶] Fault trees have been used in the nuclear industry to identify possible sequences from the failure of a basic component in an NPP to a bigger event, such as loss of coolant accident (LOCA). An 'OR' gate in a fault tree defines the failure of the event right above the gate as the failure of one or more of the events immediately below the gate.

DOI: 10.1002/eqe

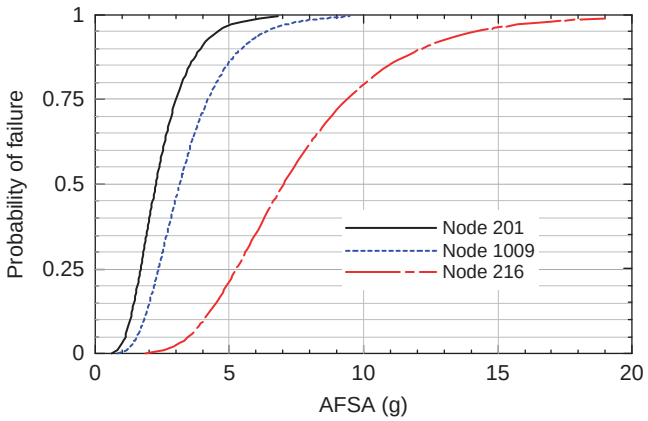

Figure 6. Fragility curves for the secondary systems at Nodes 201, 1009 and 216.

4.1. Step 2: characterize seismic hazard

This subsection presents the selection of a seismic scenario and development of ground motions for the scenario-based assessments of Models 1–4. Based on the deaggregation results presented in an Early Site Permit (ESP) report for the sample NPP site, the modal pair of moment magnitude (M_W) and closest source-to-site distance (r) at an MAFE of 10^{-5} is (5.3 and 7.5 km) for a period range between 0.1 and 0.2 s and (6.3 and 37.5 km) for a period range between 0.4 and 1 s. To investigate the governing event at periods greater than 1 s, which is not available in the ESP report, the deaggregation of the 2-s seismic hazard and a return period of 4975 years for the sample NPP site is generated using USGS interactive deaggregation tool [26] and a modal $M_W - r$ pair of (7.3 and 538 km) was identified.[‖] More information on the deaggregation results for the sample NPP site can be found in Huang *et al.* [17].

Figure 7 presents the median spectral demands predicted using the attenuation relationship of Campbell [27] for Eastern North America for the three scenario cases identified above. For clarity, panel (a) of Figure 7 presents the median spectral demands between periods of 0.01 and 1 s and panel (b) presents that between periods of 1 and 4 s. According to the information provided by the supplier of the sample NPP, the sample NPP was designed for an SSE response spectrum with a PGA higher than $0.3g$ and a spectral ordinate higher than $0.7g$ at a period of 0.04 s. The median spectral demands for the $M_W - r$ pairs of (6.3, 37.5 km) and (7.3, 538 km) are not likely to cause significant damage in the sample NPP models. The worst-case scenario, namely, the magnitude–distance pair of (5.3, 7.5 km), is selected for the scenario-based assessment of Models 1–4.

The solid curves of Figure 8 present the median, 84th and 16th percentiles of spectral accelerations predicted by Campbell [27] for the $M_W - r$ pair of (5.3, 7.5 km). The median and logarithmic standard deviation of the spectral demand for the $M_W - r$ pair at a period of 0.14 s are $0.62g$ and

[‖]The USGS interactive deaggregation tool [26] did not provide information for a return period greater than 4975 years at the time this study was performed but did show that the modal events of the 2-s hazard at return periods of 975, 2475 and 4975 years at the sample NPP site are the same. Since the purpose is to identify an important magnitude–distance combination for the 2-s hazard at the sample NPP site, the modal event of 7.3 and 538 km is used although the return period of 4975 years is much smaller than 100 000 years.

DOI: 10.1002/eqe

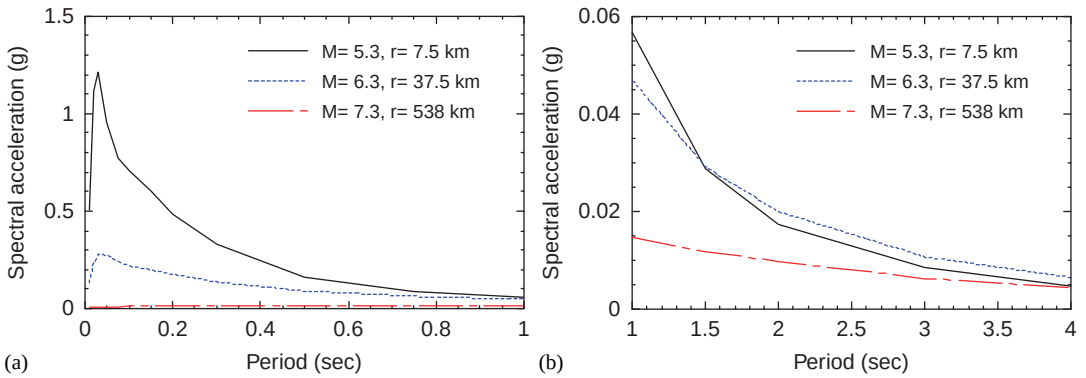

Figure 7. Median spectral accelerations predicted by Campbell [27] for three magnitude–distance pairs: (5.3, 7.5 km), (6.3, 37.5 km) and (7.3 and 538 km): (a) short-period range and (b) long-period range.

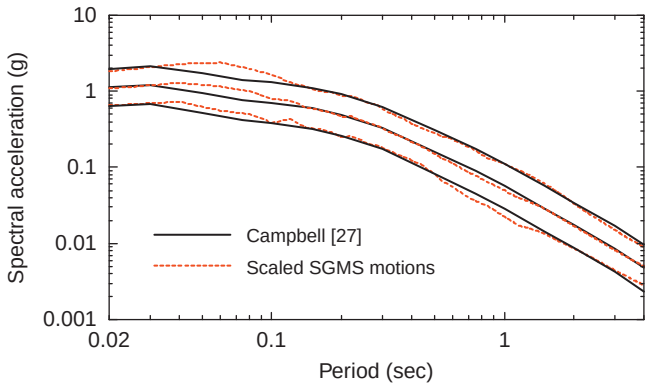

Figure 8. Median, 84th and 16th percentiles (a) of spectral accelerations predicted by Campbell [27] for $M = 5.3$ and $r = 7.5$ km and (b) of the 11-scaled SGMS ground motions of Figure 9.

0.62, respectively. Eleven target spectral ordinates at a period of 0.14 s are determined using the following equation:

$$S_{ai}(T = 0.14\,\mathrm{s}) = 0.62 \cdot \mathrm{e}^{0.62\Phi^{-1}(P_i)}, \quad i = 1, 11 \tag{2}$$

where Φ^{-1} is the inverse standardized normal cumulative distribution function and P_i is equal to $(i - 0.5)/11$. The 11 target spectral ordinates are listed in Table III and illustrated in Figure 9 using the symbol '⊛'. The technical basis for the scaling method of (2) and the use of 11 ground motions can be found in Huang *et al.* [28], which prove that the scaling method can provide unbiased estimates of median nonlinear structural responses and preserve the dispersion in the responses to a reasonable degree.

Eleven earthquake histories are generated using the computer code 'Strong Ground Motion Simulation (SGMS)' [29] for the $M_W - r$ pair of (5.3, 7.5 km) and a rock site. The SGMS code is developed based on Specific Barrier Model. It provides a complete and self-consistent description

DOI: 10.1002/eqe

Table III. Target spectral accelerations for scenario-based assessment at a period of 0.14 s.

No.	Spectral acceleration (g)
1	0.22
2	0.31
3	0.39
4	0.45
5	0.51
6	0.62
7	0.75
8	0.85
9	0.99
10	1.23
11	1.78

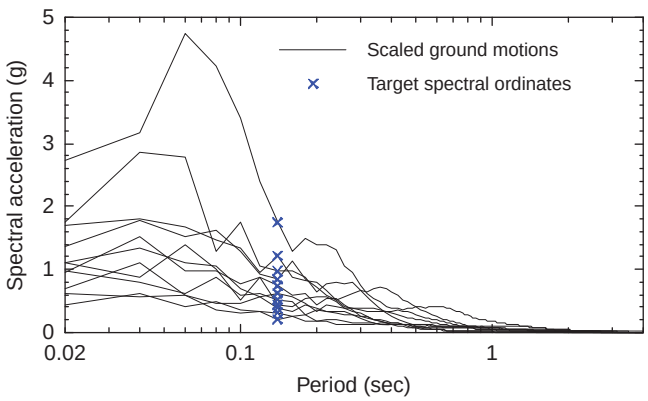

Figure 9. Spectral accelerations of the 11-scaled SGMS ground motions and the 11 target spectral ordinates for scenario-based assessment.

of the heterogeneous earthquake faulting process and can capture the rich high-frequency content in CEUS ground motions [30].

The 11 ground motions developed using SGMS are amplitude scaled to match the target spectral ordinates of Table III at a period of 0.14 s (one ground motion per target ordinate), as shown in Figure 9. The dotted curves of Figure 8 present the median, 84th and 16th percentiles of spectral accelerations of the 11-scaled SGMS ground motions. A log–log scale is used so that the results at very short period (for example, smaller than 0.1 s) or with very small spectral demand (for example, smaller than 0.1g) are clearly visible. The distribution of spectral demand of the 11-scaled SGMS ground motions agrees well with that predicted by Campbell [27] over a wide period range. This good agreement makes re-scaling of ground motions for Models 2, 3 and 4 unnecessary. The scaled ground motions of Figure 9 are used for the nonlinear response-history analyses for Models 1–4.

4.2. Step 3: simulate structural response

Nonlinear uni-directional response-history analyses are performed in SAP2000 using a direct integration algorithm for each of Models 1–4 subjected to the 11-scaled SGMS ground motions

DOI: 10.1002/eqe

of Figure 9 in the X and Y directions. Table IV presents the values of AFSA at Nodes 201, 1009 and 216 of Models 1, 2, 3 and 4 in the X direction. The results for the Y direction show a similar trend as those of Table IV and are not presented herein.

Figure 10 presents the median of the 11 floor spectral accelerations between 5 and 33 Hz and the 84th, 50th and 16th percentiles of AFSA at Node 201, where the nuclear reactor is attached to the internal structure. Again, the results at Nodes 1009 and 216 show a similar trend to those of Figure 10 and are not presented. The median ($\square$), 84th (y_{84th}) and 16th (y_{16th}) percentiles of AFSA presented in Figure 10 were computed using the following equations:

$$\square = \exp\left[\frac{1}{11}\sum_{i=1}^{11} \ln y_i\right] \tag{3}$$

$$\square = \sqrt{\frac{1}{11-1}\sum_{i=1}^{11} (\ln y_i - \ln \square)^2} \tag{4}$$

$$y_{16th} = \square \cdot e^{-\square} \tag{5}$$

$$y_{84th} = \square \cdot e^{\square} \tag{6}$$

where y_i is the ASFA value at Node 201 for a given response-history analysis. All three isolation systems analyzed herein greatly reduce the median floor spectral acceleration and AFSA demands of the sample NPP. For the AFSA demand, both the median and the difference between 84th and 16th percentiles are greatly reduced by the isolation systems. One important issue for the seismic design of secondary systems for NPPs in the CEUS is the significant high-frequency spectral demand. The results of Table IV and Figure 10 clearly show that this issue can be effectively attenuated using base isolation.

The results of the response-history analyses for each model are assembled in an 11×6 AFSA matrix, where the first three columns are those presented in Table IV for a given model in the X direction and the other three columns are for the AFSA results in the Y direction. The number of row vectors of the AFSA matrix, termed a demand-parameter matrix hereafter, is determined by the number of response-history analyses performed for a model.

The methodology of Figure 1 uses Monte-Carlo-type procedure to determine the damage state of a structural or nonstructural component (see Section 4.3). The procedure requires a large set of simulations so that the probability and annual frequency of unacceptable performance can be estimated with high confidence.

Yang *et al.* [31] provide a procedure to increase the number of row vectors in a demand-parameter matrix without performing additional response-history analysis and the resultant matrix is statistically consistent to the underlying matrix. The procedure of Yang *et al.* [31] is used in this study to increase the number of row vectors in the demand-parameter matrix from 11 to 2000. Sample results are presented in Figure 11, where the distributions of AFSA in the X direction at Nodes 201 and 1009 obtained from the underlying 11×6 matrix and the 2000×6 matrix generated per Yang *et al.* [31] are presented for Models 1–4. The AFSA values generated per the Yang *et al.* procedure preserve the magnitude and correlation in AFSA obtained using response-history analysis.

In Figure 11, significant reductions in the response space defined by the AFSA values at Nodes 201 and 1009 can be identified for the base-isolated models. The response of Model 2 is greater

DOI: 10.1002/eqe

Table IV. AFSA at Nodes 201, 1009 and 216 in the *X* direction for the scenario-based assessments of Models 1, 2, 3 and 4.

	Model 1			Model 2			Model 3			Model 4		
GM no.	Node 201	Node 1009	Node 216	Node 201	Node 1009	Node 216	Node 201	Node 1009	Node 216	Node 201	Node 1009	Node 216
1	0.46	0.60	1.22	0.12	0.14	0.30	0.04	0.05	0.07	0.01	0.01	0.02
2	0.54	0.74	1.39	0.10	0.13	0.23	0.04	0.05	0.07	0.01	0.01	0.02
3	0.66	1.05	1.90	0.14	0.19	0.33	0.07	0.07	0.10	0.02	0.02	0.03
4	1.05	1.47	2.86	0.17	0.21	0.40	0.09	0.10	0.14	0.03	0.03	0.05
5	0.83	1.14	2.15	0.12	0.15	0.27	0.05	0.06	0.10	0.02	0.02	0.03
6	1.22	1.80	2.93	0.17	0.21	0.39	0.08	0.08	0.11	0.03	0.03	0.04
7	1.09	1.55	2.98	0.19	0.24	0.45	0.07	0.08	0.13	0.03	0.03	0.05
8	1.43	1.88	3.64	0.22	0.24	0.45	0.10	0.13	0.23	0.04	0.04	0.08
9	2.03	2.49	4.48	0.24	0.26	0.57	0.10	0.12	0.19	0.06	0.06	0.09
10	1.74	2.48	5.02	0.19	0.24	0.47	0.09	0.11	0.17	0.04	0.04	0.07
11	3.92	4.75	8.80	0.33	0.34	0.77	0.16	0.17	0.30	0.08	0.08	0.14

DOI: 10.1002/eqe

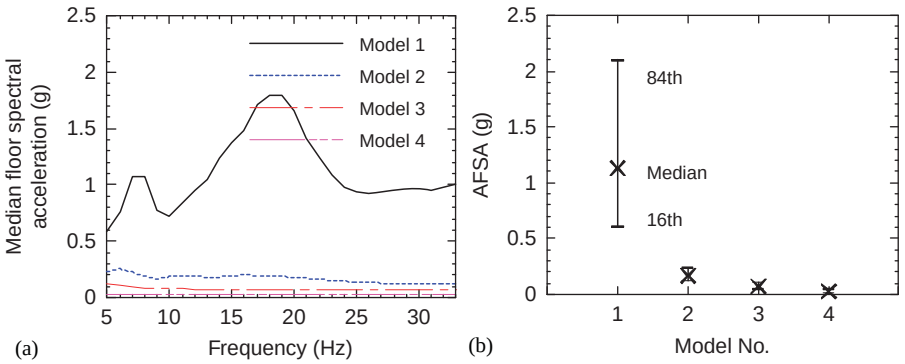

Figure 10. Floor spectral accelerations at Node 201 in the *X* direction for the scenario-based assessments of Models 1, 2, 3 and 4: (a) median floor spectral accelerations and (b) AFSA.

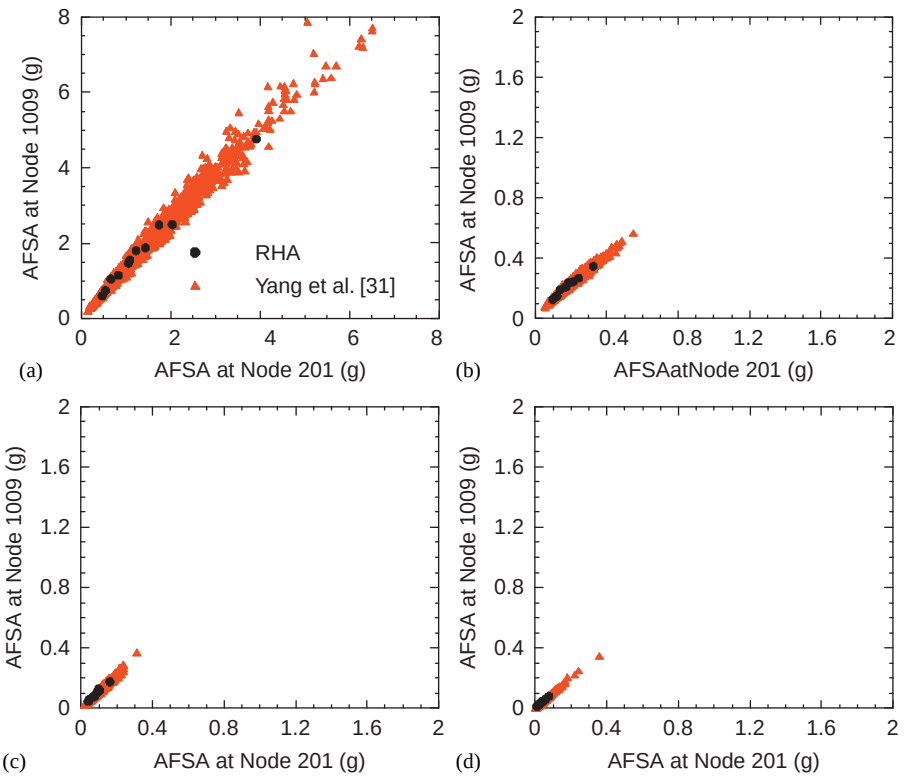

Figure 11. AFSA at Nodes 201 and 1009 in the *X* direction generated using (1) response-history analyses and (2) the procedure of Yang *et al.* [31] for the scenario-based assessments of Models 1, 2, 3 and 4: (a) Model 1; (b) Model 2; (c) Model 3; and (d) Model 4.

DOI: 10.1002/eqe

than that of Models 3 and 4 in this case. Note that the isolation system of Model 2 has higher pre-yield stiffness than those of Models 3 and 4.

4.3. Step 4: assess component damage

For each AFSA value in a row vector of the 2000×6 demand-parameter matrix, the damage state of a secondary system is determined from the corresponding fragility curve using the following steps: (1) a random number is generated using a generator that produces uniformly distributed random numbers between 0 and 1; (2) if the generated number is smaller than or equal to the probability of failure identified from the fragility curve at the given AFSA, the secondary system is considered to have failed and (3) if the generated number is greater than the probability of failure, the secondary system is considered to have passed (i.e. safe). If any of the six AFSA values in a row vector is associated with the failure of a secondary system, the performance of the NPP is considered unacceptable for this row vector.

4.4. Step 5: compute the probability of unacceptable performance

For a given model, the analysis of Section 4.3 is performed for each row vector in the 2000×6 demand-parameter matrix. The probability of unacceptable performance for the model subjected to the ground motions of Figure 9 is determined by the ratio of the number of row vectors with unacceptable performance to 2000. For Model 1, the probability of unacceptable performance is 0.51. For Models 2, 3 and 4, no unacceptable performance is observed. This does not mean that the probabilities of unacceptable performance for Models 2, 3 and 4 are zero since the probability of failure defined by any fragility curve of Figure 6 is not zero unless the value of ASFA is zero. When the probability of unacceptable performance is much smaller than 0.0005 $(=\frac{1}{2000})$, many additional trials (row vectors) are required to capture such a small probability. To investigate this further, the analysis described above is repeated using 200 000 row vectors for Models 2, 3 and 4. Only one row vector for Model 2 resulted in unacceptable performance. Accordingly, the probability of unacceptable performance for the scenario-based assessments of Models 2, 3 and 4 is smaller than 5×10^{-6}.

For those secondary systems whose design is controlled by seismic demands, the use of base isolation can reduce their construction cost by enabling design for smaller seismic lateral forces and deformations, while maintaining a probability of unacceptable performance that is equal to or smaller than that in conventional NPPs. To quantify the possible percentage reduction in the required lateral strength of a secondary component or system, a parameter, R_a, is defined as

$$R_a = \frac{\hat{a}'}{\hat{a}} \tag{7}$$

where $\hat{a}$ and $\hat{a}'$ are the original and *reduced* median values of the fragility curves of interest. In this study, $\hat{a}$ are 2.26, 3.15 and $7.02g$ for the three fragility curves of Figure 6 and R_a is varied between 0.01 and 1.

The analysis described above is repeated for each of Models 2, 3 and 4 using the demand-parameter matrix with 2000 row vectors** and the updated fragility curves, where the median

**This analysis was also performed using demand-parameter matrixes with 200 000 row vectors and the result is nearly identical to that of Figure 12. If the median values of the fragility curves are reduced, the probability of unacceptable performance increases and the use of a very large number of row vectors is unnecessary.

DOI: 10.1002/eqe

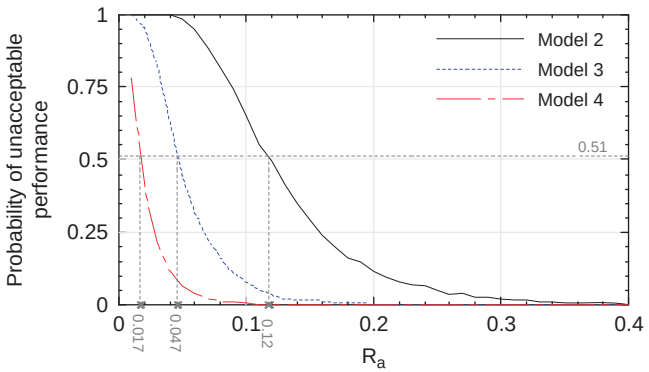

Figure 12. Probability of unacceptable performance as a function of R_a for the scenario-based assessments of Models 2, 3 and 4.

capacity for each fragility curve of Figure 6 is reduced from $\hat{a}$ to $R_a\hat{a}$. The results are presented in Figure 12 as a function of R_a and model number, together with the probability of unacceptable performance for Model 1 and the value of R_a for each isolated NPP model that has a probability of unacceptable performance equal to that for Model 1.

The values of R_a for the *equivalent* performance in Figure 12 are 0.12, 0.047 and 0.017 for Models 2, 3 and 4, respectively. Although such small values of R_a likely have little practical significance since seismic demand is not the only factor controlling the design of a secondary system, these results show the advantages of base isolation, namely, enabling the design of secondary systems for far smaller seismic demands than for those in conventional NPPs.

5. TIME-BASED ASSESSMENT

5.1. Step 2: characterize seismic hazard

A time-based assessment is performed as a series of intensity-based assessments with target spectral ordinates characterized using a seismic hazard curve over a wide range of MAFE. Figures 13 and 14 present the seismic hazard curves used in the time-based assessment, which were developed for periods of 0.14 and 2 s, respectively, based on the results of probabilistic seismic hazard analysis (PSHA) presented in the ESP report. The hazard curve of Figure 13 is for the assessment of Model 1 and that of Figure 14 is for the assessments of Models 2, 3 and 4. More information on the development of these hazard curves can be found in Huang *et al.* [17].

Figure 13 illustrates the computation of the target spectral ordinates for scaling ground motions for the time-based assessment of Model 1. The range of spectral acceleration is selected as 0.05–2.68g, where the lower- and upper-bound spectral ordinates are associated with MAFEs of 1.43×10^{-3} and 1.0×10^{-6}, respectively. The lower bound of 0.05g is selected since such a ground motion is unlikely to cause any damage in the sample NPP; the upper bound is selected since it is associated with a smallest MAFE available in the ESP report. The range of spectral acceleration is split into eight equal intervals ($\square e_1$ to $\square e_8$ of Figure 13) and the midpoint value in each interval identifies a target spectral demand for the scaling of ground motions. The eight

DOI: 10.1002/eqe

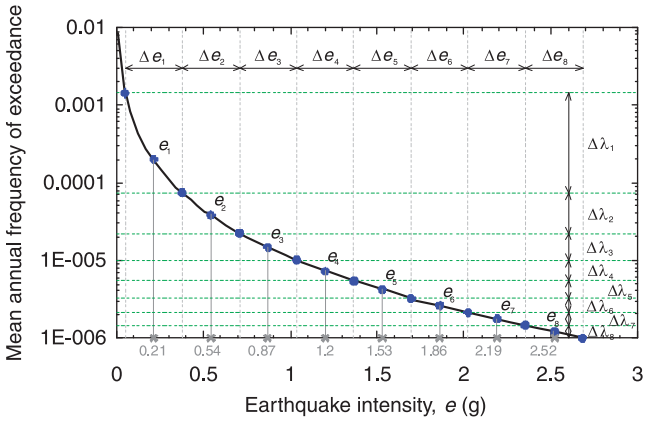

Figure 13. Computation of target spectral ordinates for the time-based assessment of Model 1.

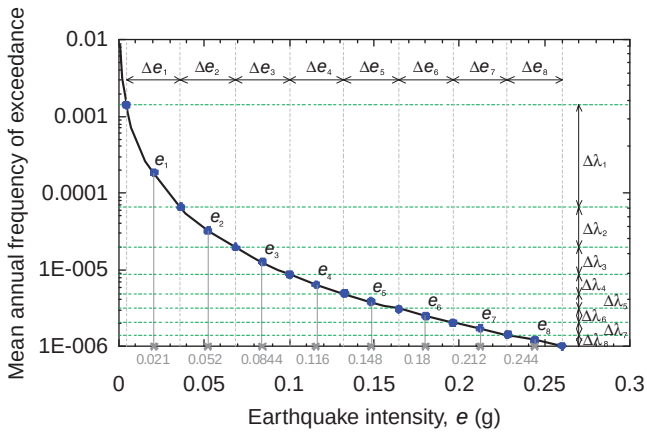

Figure 14. Computation of target spectral ordinates for the time-based assessments of Models 2, 3 and 4.

target spectral ordinates are identified in the figure by the symbol '⊛' with values of 0.21, 0.54, 0.87, 1.2, 1.53, 1.86, 2.19 and 2.52g. The mean annual frequency (MAF, $\square\square_i$) associated with each spectral interval is computed as the difference in the MAFEs at the boundaries of the interval and presented in the second column of Table V.

Eight bins of ground motions, termed Bins TC1–TC8, used in the time-based assessment of Model 1 are developed by amplitude scaling the 11 SGMS ground motions described in Section 4.1 to each of the eight target spectral ordinates identified in Figure 13 at a period of 0.14 s.

The analysis of Figure 13 is repeated using the 2-s hazard curve of Figure 14 to determine the target spectral ordinates for scaling ground motions for the time-based assessments of Models 2, 3 and 4. To enable a comparison, the MAFE range for Model 1 (1.43×10^{-3} to 1.0×10^{-6}) is also used in Figure 14. The eight target spectral ordinates are identified on the X axis of Figure 14 by the symbol '⊛' with values of 0.021, 0.052, 0.0844, 0.116, 0.148, 0.18, 0.212 and 0.244g. The values of $\square\square_i$ for the eight spectral intervals are listed in the second column of Table VI. Eight

DOI: 10.1002/eqe

Table V. Computation of annual frequency of unacceptable performance of Model 1 using 2000 row vectors.

Ground-motion bin	□□$_i$	Probability of unacceptable performance, P_i	□□$_i \times P_i$
TC1	1.35E−03	0	0
TC2	5.18E−05	0.16	8.29E−06
TC3	1.24E−05	0.68	8.43E−06
TC4	4.63E−06	0.94	4.35E−06
TC5	2.23E−06	0.99	2.21E−06
TC6	1.08E−06	1	1.08E−06
TC7	6.90E−07	1	6.90E−07
TC8	4.59E−07	1	4.59E−07
Annual frequency of unacceptable performance	□$_{i=1}^{8}$ □□$_i \times P_i$		2.55E−05

Table VI. Computation of annual frequency of unacceptable performance of Models 2, 3 and 4 using 200 000 row vectors.

		Probability of unacceptable performance, P_i			□□$_i \times P_i$		
Ground-motion bin	□□$_i$	Model 2	Model 3	Model 4	Model 2	Model 3	Model 4
TI1	1.35E−03	0	0	0	0	0	0
TI2	4.57E−05	2.00E−05	0	0	9.15E−10	0	0
TI3	1.07E−05	6.00E−05	0	0	6.42E−10	0	0
TI4	3.85E−06	1.30E−04	0	0	5.00E−10	0	0
TI5	1.87E−06	2.15E−04	0	0	4.02E−10	0	0
TI6	1.03E−06	3.85E−04	0	5.00E−06	3.96E−10	0	5.14E−12
TI7	6.09E−07	4.90E−04	2.00E−05	1.05E−04	2.98E−10	1.22E−11	6.39E−11
TI8	4.05E−07	7.75E−04	7.50E−05	2.35E−04	3.13E−10	3.03E−11	9.51E−11
Annual frequency of unacceptable performance					3.47E−09	4.25E−11	1.64E−10

bins of ground motions, termed as Bins TI1–TI8, used in the time-based assessment for Models 2, 3 and 4 were developed by amplitude scaling the 11 SGMS ground motions of Section 4.1 to each of the eight target spectral ordinates identified in Figure 14 at a period of 2 s.

5.2. Step 3: simulate structural response

Unidirectional nonlinear response-history analyses are performed for Model 1 subjected to the Bins TC1–TC8 ground motions and Models 2, 3 and 4 subjected to the Bins TI1–TI8 ground motions in the X and Y directions. The response-history analysis for each model and each bin of ground motions produced an 11×6 demand-parameter matrix, where each row includes the ASFA values at Nodes 206, 1009 and 216 in the X and Y directions for each ground motion in the bin.

Panels (a) and (b) of Figure 15 present the medians (□) and logarithmic standard deviations (□), respectively, of the AFSA values at Node 201 in the X direction as a function of ground-motion bin. The values of □ and □ are computed using (3) and (4). Note that for a given bin number in Figure 15, the ground-motion bin used in the analysis for Model 1 (Bin TCi) is different from that used in the analysis for Models 2, 3 and 4 (Bin TIi).

An advantage of the implementation of base isolation can be observed in Figure 15: as the intensity of the earthquake shaking increases, the increase in the AFSA response in the base-isolated NPPs is much smaller than that in the conventional NPP. In panel (a) of Figure 15, the

DOI: 10.1002/eqe

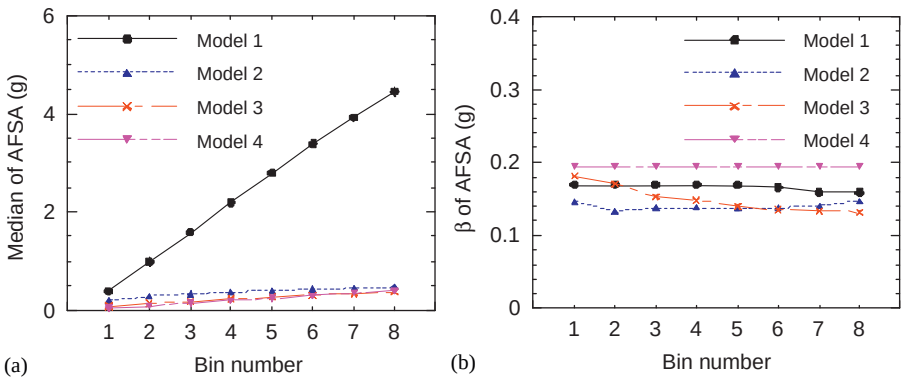

Figure 15. Median and of AFSA at Node 201 in the *X* direction as a function of ground-motion bin for the time-based assessments of Models 1, 2, 3 and 4: (a) median and (b) Model 4.

median AFSAs for Model 1 subjected to the ground motions of Bins TC1 and TC8 are 0.38 and 4.45*g*, respectively; and those for Model 2 subjected to the ground motions of Bins TI1 and TI8 are 0.20 and 0.48*g*, respectively. This observation explains why, for scenario-based assessment, the dispersion in AFSA for the conventional NPP model is much greater than that for the nonlinear base-isolated NPPs: the ground motions used in scenario-based assessment are scaled to cover a wide range of spectral accelerations at the fundamental period of the structure and the increase of AFSA due to the increase of the spectral acceleration is much greater in the conventional NPP than in the base-isolated NPPs.

Figure 15(b) shows that the dispersion () in AFSA for the conventional NPP is not necessarily higher or lower than that for the base-isolated NPPs when the ground motions are scaled to a given spectral acceleration at a given period. The dispersion for Model 4 is a constant since the isolation system is modeled as a linear spring and an LVD and the superstructure does not yield in this case. Of the four models, the value of for Model 3, which is the NPP equipped with LR bearings, is the most sensitive to the earthquake intensity and the value of decreases as the intensity of earthquake increases.

For each of the eight 11×6 demand-parameter matrices for Model 1 (Models 2, 3 and 4), 2000 (200 000) row vectors are generated using the procedure of Yang *et al.* [31]. The new matrix composed of the resultant row vectors is statistically consistent with the underlying matrix and used in Steps 4 and 5 to compute the probability of unacceptable performance for each ground-motion bin.

5.3. Steps 4 and 5: assess component damage and compute the annual frequency of unacceptable performance

The procedure of Section 4.3 is used to determine the probability of unacceptable performance for each 2000×6 or $200\,000\times6$ demand-parameter matrix developed in Section 5.2. For a given model, the product of the probability of unacceptable performance for each ground-motion bin (P_i) and the MAF associated with the bin ($_i$) is computed. The sum of the eight products is defined as the annual frequency of unacceptable performance for the model.

The results of P_i, $_i \times P_i$ and the annual frequency of unacceptable performance for Model 1 are presented in Table V and those for Models 2, 3 and 4 are presented in the Table VI. Bins of ground motions with lower spectral demand occur more frequently but have a lower probability

DOI: 10.1002/eqe

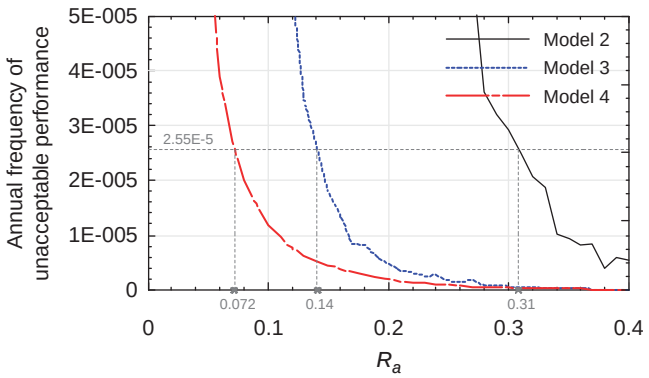

Figure 16. Annual frequency of unacceptable performance as a function of R_a for Models 2, 3 and 4.

of unacceptable performance than bins of motions with higher spectral demand: see the values of $\square\square_i$ and P_i in Tables V and VI. The time-based assessment systematically incorporates $\square\square_i$ and P_i to compute the MAF of unacceptable performance. The MAFs of unacceptable performance of Models 2, 3 and 4 are 3.47×10^{-9}, 4.25×10^{-11} and 1.64×10^{-10}, respectively, and much smaller than that of Model 1 (2.55×10^{-5}).

The analyses of Figure 12 are repeated using the AFSA results for the time-based assessments of Models 2, 3 and 4 to characterize the relationship between R_a and the annual frequency of unacceptable performance. The analyses were performed using 2000 row vectors.[††] The results are presented in Figure 16 as a function of R_a and models. Figure 16 also presents the annual frequency of unacceptable performance identified in Table V for Model 1 and the value of R_a for each isolated NPP model that has an annual frequency of unacceptable performance equal to that for Model 1. The values of R_a for this equivalent performance are 0.31, 0.14 and 0.072 for Models 2, 3 and 4, respectively. The results of Figure 16 show that the use of base isolation systems enables secondary systems to be designed for smaller strengths than those in conventional NPPs and to achieve a lower annual frequency of unacceptable performance than that in a conventional NPP.

6. CONCLUSIONS

The seismic performance of sample conventional and base-isolated NPP reactor buildings is assessed for a rock site in the Eastern U.S. Key secondary systems in the sample reactor building were identified. The demand parameter controlling the response of these systems was assumed to be floor spectral acceleration. Unacceptable performance was defined as the failure of any of the key secondary systems. The key conclusions of these assessments are:

1. The assessment methodology used in this paper can be applied to intensity-, scenario- and time-based assessments to evaluate the probability and annual frequency of unacceptable

[††]Another set of analyses similar to that presented herein but using 20 000 row vectors was performed to ensure that the use of 2000 row vectors was sufficient. The results for 20 000 row vectors are almost identical to those for 2000 row vectors.

DOI: 10.1002/eqe

performance of an NPP for a given seismic hazard. It can be used to evaluate the seismic performance of both conventional and base-isolated NPPs. A key issue is the selection and scaling of ground motions for different types of assessment. For scenario-based assessment, the dispersion in the spectral accelerations for a given $M_W - r$ pair should be appropriately addressed. For time-based assessment, a wide range of earthquake intensity should be covered.

2. The use of base isolation improves the seismic performance (or reduces risk or vulnerability) of the sample NPP reactor building by many orders of magnitude. In the scenario-based assessment for a $M_W - r$ pair of (5.3, 7.5 km), the probability of unacceptable performance for the conventional reactor building is 0.51 and that for the base-isolated reactor buildings is smaller than 5×10^{-6}. For the time-based assessment, the annual frequency of unacceptable performance for the conventional reactor building is 2.55×10^{-5} and that for the base-isolated reactor buildings is smaller than 4×10^{-9}.
3. The use of base isolation greatly reduces the seismic demand on the secondary systems. In the scenario-based assessment, the median seismic capacities of the secondary systems for the base-isolated models could be reduced by at least 88% to achieve a probability of unacceptable performance equal to that for the conventional model. In the time-based assessment, the corresponding reduction is 69% to achieve an annual frequency of unacceptable performance equal to that for the conventional NPP. Although these percentages likely have little practical significance since the design of the secondary systems would be controlled by other demands for such a circumstance, these results show the advantage of base isolation, namely, enabling a more economical design of secondary systems than in the conventional NPPs. The reduction in cost of key secondary systems will offset the increased construction cost associated with the seismic isolators and related structural framing.
4. As the intensity of earthquake shaking increases, the increase in the demands for structural and nonstructural components in the base-isolated NPPs is much smaller than that in the conventional NPP: an observation that enables the standardization for the design of structural and secondary components and systems in base-isolated NPPs at different sites.
5. For base-isolated NPPs, the reduction in AFSA for secondary components and systems to below $1g$ could reduce or eliminate the need for seismic qualification at certain sites across the U.S. because all components and systems must function in a $1g$ gravity field.

ACKNOWLEDGEMENTS

The research presented in this paper was supported in part by MCEER (www.mceer.buffalo.edu) through grants from the Earthquake Engineering Centers Program of the National Science Foundation, Award Number EEC-9701471, and the State of New York. The opinions expressed in the paper are those of the authors and do not reflect the views of the sponsors or the Research Foundation of the State University of New York. No guarantee regarding the results, findings and recommendations is offered by MCEER, the National Science Foundation or the State of New York.

REFERENCES

1. Naeim F, Kelly JM. *Design of Seismic Isolated Structures*: *From Theory to Practice*. Wiley: NY, 1999.
2. Constantinou MC, Whittaker AS, Kalpakidis Y, Fenz DM, Warn GP. Performance of seismic isolation hardware under service and seismic loading. *MCEER-07-0012*, Multidisciplinary Center for Earthquake Engineering Research, State University of New York, Buffalo, NY, 2007.

DOI: 10.1002/eqe

3. Eidinger JM, Kelly JM. Seismic isolation for nuclear power plants: technical and non-technical aspects in decision making. *Nuclear Engineering and Design* 1985; **84**(3):383–409.
4. Bhatti MA, Ciampi V, Kelly JM, Pister KS. An earthquake isolation system for steam generators in nuclear power plants. *Nuclear Engineering and Design* 1982; **73**(3):229–252.
5. Kelly JM, Tsai HC. Seismic response of light internal equipment in base-isolated structures. *Report No. UCB/SESM-84/17*, Division of Structural Engineering and Structural Mechanics, Department of Civil Engineering, College of Engineering, University of California, Berkeley, CA, 1984.
6. Fan FG, Ahmadi G. Seismic responses of secondary systems in base-isolated structures. *Engineering Structures* 1992; **14**(1):35–48.
7. Khechfe H, Noori M, Hou Z, Kelly JM, Ahmadi G. An experimental study on the seismic response of base-isolated secondary systems. *Journal of Pressure Vessel Technology* (ASME) 2002; **124**(1):81–88.
8. Huang YN, Whittaker AS, Constantinou MC, Malushte S. Seismic demands on secondary systems in isolated nuclear power plants. *Earthquake Engineering and Structural Dynamics* 2007; **36**(12):1741–1761.
9. U.S. Nuclear Regulatory Commission (USNRC). Individual plant examination of external events (IPEEE) for severe accident vulnerabilities. *Generic Letter No. 88-20*, *Supplement 4*, U.S. Nuclear Regulatory Commission, Washington, DC, 1991.
10. Chen JT, Chokshi NC, Kenneally RM, Kelly GB, Beckner WD, McCracken C, Murphy AJ, Reiter L, Jeng D. Procedural and submittal guidance of individual plant examination of external events (IPEEE) for severe accident vulnerabilities. *NUREG-1407*, U.S. Nuclear Regulatory Commission, Washington, DC, 1991.
11. Budnitz RJ, Amico PJ, Cornell CA, Hall WJ, Kennedy RP, Reed JW, Shinozuka M. An approach to the quantification of seismic margins in nuclear power plants. *NUREG/CR*-4334, U.S. Nuclear Regulatory Commission, Washington, DC, 1985.
12. Prassinos PG, Ravindra MK, Savy JB. Recommendations to the Nuclear Regulatory Commission on trial guidelines for seismic margin reviews of nuclear power plants. *NUREG/CR-4482*, U.S. Nuclear Regulatory Commission, Washington, DC, 1986.
13. Reed JW, Kennedy RP, Buttemer DR, Idriss IM, Moore DP, Barr T, Wooten KD, Smith JE. A methodology for assessment of nuclear power plant seismic margin (revision 1). *NP-6041-SL*, Electric Power Research Institute, Palo Alto, CA, 1991.
14. Smith PD, Dong RG, Bernreuter DL, Bohn MP, Chuang TY, Cummings GE, Johnson JJ, Mensing RW, Wells JE. Seismic safety margins research program: phase 1 final report. *NUREG/CR-2015*, U.S. Nuclear Regulatory Commission, Washington, DC, 1981.
15. U.S. Nuclear Regulatory Commission (USNRC). PRA procedures guide. *NUREG/CR-2300*, U.S. Nuclear Regulatory Commission, Washington, DC, 1983.
16. Reed JW, Kennedy RP. Methodology for developing seismic fragilities. *TR-103959*, Electric Power Research Institute, Palo Alto, CA, 1994.
17. Huang YN, Whittaker AS, Luco N. Performance assessment of conventional and base-isolated nuclear power plants for earthquake and blast loadings. *MCEER-08-0019*, Multidisciplinary Center for Earthquake Engineering Research, State University of New York, Buffalo, NY, 2008.
18. Computers and Structures, Inc. (CSI). SAP2000 linear and nonlinear static and dynamic analysis and design of three-dimensional structures—version 11.0. Computers and Structures, Inc., Berkeley, CA, 2006.
19. Wood SL. Shear strength of low-rise reinforced concrete walls. *ACI Structural Journal* 1990; **87**(1):99–107.
20. Constantinou MC, Tsopela P, Kasalanati A, Wolff ED. Property modification factors for seismic isolation bearings. *MCEER-99-0012*, Multidisciplinary Center for Earthquake Engineering Research, State University of New York, Buffalo, NY, 1999.
21. Fenz DM. Further development, testing and modeling of the Axon seismic isolation system. *Master Thesis*, Department of Civil, Structural and Environmental Engineering, State University of New York, Buffalo, NY, 2005.
22. Kalpakidis IV, Constantinou MC. Effects of heating on the behavior of lead–rubber bearings. I: theory. *Journal of Structural Engineering* 2009; **135**(12):1440–1449.
23. Kalpakidis IV, Constantinou MC. Effects of heating on the behavior of lead–rubber bearings. II: verification of theory. *Journal of Structural Engineering* 2009; **135**(12):1450–1461.
24. Huang YN, Whittaker AS, Kennedy RP, Mayes RL, Assessment of base-isolated nuclear structures for design and beyond-design basis earthquake shaking. *MCEER-09-0008*, Multidisciplinary Center for Earthquake Engineering Research, State University of New York, Buffalo, NY, 2009.
25. Kennedy RP, Ravindra MK. Seismic fragilities for nuclear power plant risk studies. *Nuclear Engineering and Design* 1984; **79**(1):47–68.

DOI: 10.1002/eqe

26. U.S. Geological Survey (USGS). 2002 interactive deaggregations. Available from: http://eqint.cr.usgs.gov/deaggint/2002/index.php [1 September 2008].
27. Campbell KW. Prediction of strong ground motion using the hybrid empirical method and its use in the development of ground-motion (attenuation) relations in Eastern North America. *Bulletin of the Seismological Society of America* 2003; **93**(3):1012–1033.
28. Huang YN, Whittaker AS, Luco N, Hamburger RO. Scaling earthquake ground motions for performance-based design. *Journal of Structural Engineering* 2009; DOI: 10.1061/(SACE)ST.1943-541X.0000155.
29. Halldorsson B. Strong Ground Motion Simulation (SGMS) code. Engineering Seismology Laboratory, State University of New York, Buffalo, NY. Available from: http://civil.eng.buffalo.edu/engseislab/products.htm [1 September 2004].
30. Halldorsson B, Papageorgiou AS. Calibration of the specific barrier model to earthquakes of different tectonic regions. *Bulletin of the Seismological Society of America* 2005; **93**(3):1099–1131.
31. Yang TY, Moehle JP, Stojadinovic B, Der Kiureghian A. Seismic performance evaluation of facilities: methodology and implementation. *Journal of Structural Engineering* 2009; **135**(10):1146–1154.

DOI: 10.1002/eqe